

# Efficiency Improvement of Organic Solar Cells via Introducing Combined Anode Buffer Layer To Facilitate Hole Extraction

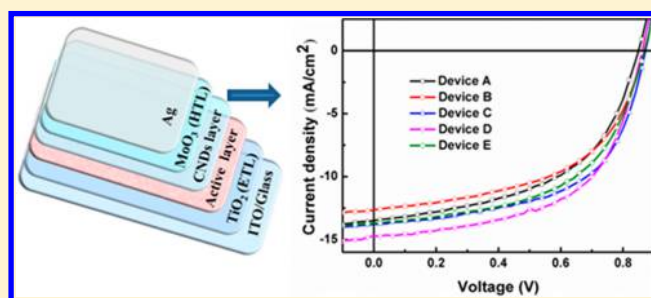
Xinyuan Zhang,<sup>†</sup> Zhiqi Li,<sup>†</sup> Zhihui Zhang,<sup>†</sup> Shujun Li,<sup>§</sup> Chunyu Liu,<sup>†</sup> Wenbin Guo,<sup>\*,†</sup> Liang Shen,<sup>†,‡</sup> Shanpeng Wen,<sup>†</sup> Songnan Qu,<sup>§</sup> and Shengping Ruan<sup>\*,†</sup>

<sup>†</sup>State Key Laboratory on Integrated Optoelectronics, College of Electronic Science and Engineering, Jilin University, 2699 Qianjin Street, Changchun 130012, China

<sup>‡</sup>Department of Mechanical and Materials Engineering and Nebraska Center for Materials and Nanoscience, University of Nebraska–Lincoln, Lincoln, Nebraska 68588-0656, United States

<sup>§</sup>State Key Laboratory of Luminescence and Applications, Changchun Institute of Optics, Fine Mechanics and Physics, Chinese Academy of Sciences, 3888 Eastern South Lake Road, Changchun 130033, China

**ABSTRACT:** In this article, we introduce a new method to assist hole extraction by incorporating carbon nanodots (CNDs) interfacial layer between active layer and hole-transporting layer for organic solar cells (OSCs). Under an optimal concentration of CNDs and specific film-forming conditions, a simultaneous enhancement of short-circuit current density ( $J_{sc}$ ) and fill factor (FF) was achieved, leading to the optimal power conversion efficiency up to 7.22%. Due to the nice conductivity of CNDs, the interlayer effectively bridged the separated islands of active layer to transport free charge carriers toward correct electrodes and reduced charge carrier recombination. The employment of interface modification depicted here can also provide a rough and uniform surface coating on polymer photolayer, leading to improved morphology and closer interface contact, and thus reduce the series resistance and increase FF of OSCs. In addition, the incorporation of CNDs also increased the light-harvesting of active layer. Therefore, the CNDs interfacial layer could play a dual role in the improvement of optical and electrical properties for OSCs.



## 1. INTRODUCTION

Solution-processed bulk heterojunction (BHJ) organic solar cells (OSCs) based on conjugated polymer:fullerene composites have made impressive progress in the last decades and have rapidly achieved inspiring solar-to-electricity power conversion efficiencies (PCEs) of 10% for single BHJ OSCs recently, which are close to a broad commercialization.<sup>1–5</sup> Considering the power conversion processes, including solar light absorption, exciton generation and dissociation, and carriers transport and collection, generally, two feasible strategies are widely employed to improve the PCE of OSCs.<sup>6–13</sup> One is the reforming of device engineering, such as device structures, fabricating technology, and study of device mechanism.<sup>14–17</sup> The other is to design new materials with superior properties including both active and interface layer materials.<sup>18–20</sup> Through introducing near-infrared absorbers (rare-earth materials) and using plasmonic nanostructures (such as nanodots and nanohole arrays) to make the utmost use of the solar spectrum, a higher short-circuit current ( $J_{sc}$ ) has been achieved.<sup>21,22</sup> By ameliorating the morphology of the photoactive layer and adjusting the donor and acceptor (D–A) phase separation, such as thermal annealing and solvent treatment, the fill factors (FF) of OSCs have been enhanced greatly.<sup>23,24</sup> However, further improvement of the device performance such as long-time stability and low-cost are still

necessary criteria for OSCs in practical application. Given these prominent strides in active layer engineering, there now comes the chance to improve contacts and interfaces to enable further progress in efficiency of OSCs. In OSCs, the  $J$ – $V$  curve relates not only to the bulk properties of the active layer but also to the interface properties between the organic materials and the metal contacts or the charge-transport layers, which have a big influence on charge carriers transportation.<sup>25–29</sup> The main bottleneck for OSCs to achieve higher PCEs is the trade-off between efficient photogeneration of charge carriers and their collection efficiency at the respective electrodes. Inefficient charge splitting and the low conductivity within the polymer material inherently, especially the unbalanced carrier mobilities of electrons ( $\sim 10^{-4}$  cm<sup>2</sup> V<sup>-1</sup> s<sup>-1</sup>) and holes ( $\sim 10^{-5}$  cm<sup>2</sup> V<sup>-1</sup> s<sup>-1</sup>), are linchpin hurdles in the development of OSCs.<sup>30</sup> When the mobility of two kinds of carriers differs over 2 orders of magnitude, a too-low hole mobility most likely leads to building up space-charge in the devices and leads to inferior FF and PCE for OSCs.<sup>31</sup> Therefore, intrinsically improving charge transport especially hole transfer and extraction capacity in OSCs, such as engineering and modification of interface between the photo-

Received: April 11, 2016

Revised: June 10, 2016

Published: June 15, 2016

active layer and buffer layer or metal electrodes, offers a promising way to achieve better performance.<sup>32–34</sup> Moreover, OSCs are generally stacked with thin films architecture, and the performance critically relies on the properties of interfaces between distinct materials, such as extracting and collecting charge carriers from the interface of organic active layer and transition metal oxide transport layer.<sup>35–37</sup>

In this research, we demonstrated an improvement of the hole extraction for OSCs by incorporating carbon nanodots (CNDs) interfacial layer between the buffer layer and the active layer. Poly[*N*-9''-hepta-decanyl-2,7-carbazolealt-5,5-(4',7'-di-2-thienyl-2',1',3'-benzothiadiazole)] (PCDTBT) and fullerene derivative [6,6]-phenyl-*C*<sub>71</sub>-butyric acid methylester (PC<sub>71</sub>BM) were used as active layer materials. In place of the conventional structure, inverted solar cells have been adopted in our study for better device performance due to the advantages of utilizing the spontaneous vertical phase separation.<sup>38</sup> Meanwhile, the modified layer could adjust active film roughness expediently to form a ideal feature and thus contact the hole transport layer (HTL) closely. The modification was performed by spin-coating a thin film of alcohol-soluble CNDs on top of the active layer and thermal annealing subsequently, which owns fabulous conductivity. By controlling the concentration of CNDs solution, the thickness, and annealing time of modified layer, we demonstrated that the PCE of the PCDTBT:PC<sub>71</sub>BM based solar cells increased from 5.93% to 7.22% because of the improvement of  $J_{sc}$  and FF. Importantly, the hole mobility has been enhanced apparently, which could avoid recombination originating from hole accumulation; thus, hole carriers can be efficiently swept out to the electrodes, leading to the increase of photoconductivity and consequent PCEs.

## 2. DEVICE FABRICATION AND CHARACTERIZATION

The CNDs were synthesized according to refs 39 and 40, and the transmission electron microscopy (TEM) image of CNDs is shown in Figure 1, whose dimension is 2–5 nm. CNDs

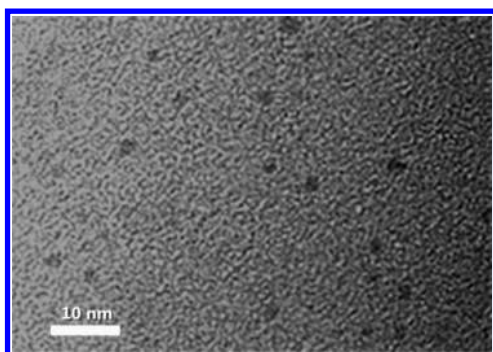


Figure 1. TEM image of CNDs used in our study.

material was dissolved in isopropyl alcohol, and the concentrations were 0.1, 0.15, and 0.2 mg/mL respectively. The inverted OSCs schematic structure of ITO (150 nm)/nc-TiO<sub>2</sub> (25 nm)/PCDTBT:PC<sub>71</sub>BM (100 nm)/CNDs/MoO<sub>3</sub> (10 nm)/Ag (100 nm) and energy level are shown in Figure 2. In the fabrication process, the ITO-conducting glass substrate was first pre-cleaned with acetone, isopropyl alcohol, and deionized water and subsequently dried with nitrogen. Anatase TiO<sub>2</sub> layer was prepared onto ITO substrate as an electron-transport layer. TiO<sub>2</sub> was spin-cast at 3000 rotations per minute (rpm) on the top of the ITO-coated glass substrates and then

thermally sintered at 450 °C for 2 h in the muffle furnace and cooled naturally. The PCDTBT:PC<sub>71</sub>BM (1:4 by weight) active layer was prepared by spin-coating with 1,2-dichlorobenzene (DCB) solution and then annealed at 70 °C for 20 min in a glovebox. All the experimental parameters were optimized on the basis of previous experience.<sup>41,42</sup> CNDs solution was prespin-cast at 800 rpm for 6 s and formal spin-cast at 2300 rpm for 18 s, and then further annealed at 70 °C for 5 min in a glovebox. The devices were completed by thermal evaporation of MoO<sub>3</sub> and Ag electrode respectively at last.<sup>43,44</sup> MoO<sub>3</sub> was selected as HTL due to the high work function (5.3 eV), which has potential to improve hole collection. The fabricated cells with different concentrations of 0.1, 0.15, and 0.2 mg/mL CNDs interlayer are named as Device C, Device D, and Device E. Also, the devices with structure of ITO/nc-TiO<sub>2</sub>/PCDTBT:PC<sub>71</sub>BM/MoO<sub>3</sub>/Ag and ITO/nc-TiO<sub>2</sub>/PCDTBT:PC<sub>71</sub>BM/isopropyl alcohol/MoO<sub>3</sub>/Ag were fabricated as reference, which were named Device A and Device B. Every valid area of the OSC devices is about 0.064 cm<sup>2</sup>, and all measurements were carried out under ambient condition without encapsulation.

## 3. RESULTS AND DISCUSSION

Current density–voltage ( $J$ – $V$ ) characteristics of the finished devices were measured using a computer-programmed Keithley 2601 source/meter under AM1.5G solar illuminations with an Oriel 300 W solar simulator intensity of  $\sim 100$  mW cm<sup>-2</sup> (about 1 sun) in air. The light intensity was measured with a photometer (Internationallight, IL1400) corrected by a standard silicon solar cell. Figure 3a shows the  $J$ – $V$  characteristics of the fabricated devices with various concentrations of CNDs interlayer. The control device (Device A) without any modifier indicates a  $J_{sc}$  of 13.49 mA cm<sup>-2</sup>, an open-circuit voltage ( $V_{oc}$ ) of 0.85 V, and a FF of 51.74%, leading to a PCE of 5.93%, which is at the same level of reported inverted BHJ-OSC devices fabricated under similar conditions.<sup>45</sup> After CNDs were incorporated between active layer and MoO<sub>3</sub>, the performance of the modified devices improved remarkably. Under an optimal modification, the PCE of Device D is 7.22% including a  $J_{sc}$  of 14.71 mA cm<sup>-2</sup>, a  $V_{oc}$  of 0.86 V, and a FF of 56.93%.  $J_{sc}$  and FF were both optimized, which explicitly resulted in a 21.74% enhancement of PCE compared to Device A. Moreover, Device C and Device E were also conducted, and they also shown relatively higher PCEs than control devices, exhibiting PCEs of 6.84% and 6.51%.  $J_{sc}$  and FF are all ameliorated for the CNDs modified devices independent of concentration without the change of  $V_{oc}$ .

With the increase of CNDs concentration, PCE of modified devices has an obvious change trend, which rises first and then decreases.  $V_{oc}$  of all devices maintained same level with almost imperceptible fluctuation, which may arise from changes in interfacial band bending after modification, suggesting that CNDs thin film has little influence on the energy levels distribution of cells. As is well-known,  $V_{oc}$  of OSCs is principally decided by the energy difference between the highest occupied molecular orbital (HOMO) and the lowest unoccupied molecular orbital (LUMO) of D–A materials.<sup>46,47</sup> The introduction of CNDs interlayer did not take a heavy toll on homogeneous D–A phase, but rather connected isolated islets of the net, forming efficient pathways for charge transport. The changes of the work function (WF) induced by CNDs interlayer were measured by a Kelvin probe system (KP 6500 Digital Kelvin probe, McAllister Technical Services Co., Ltd.).

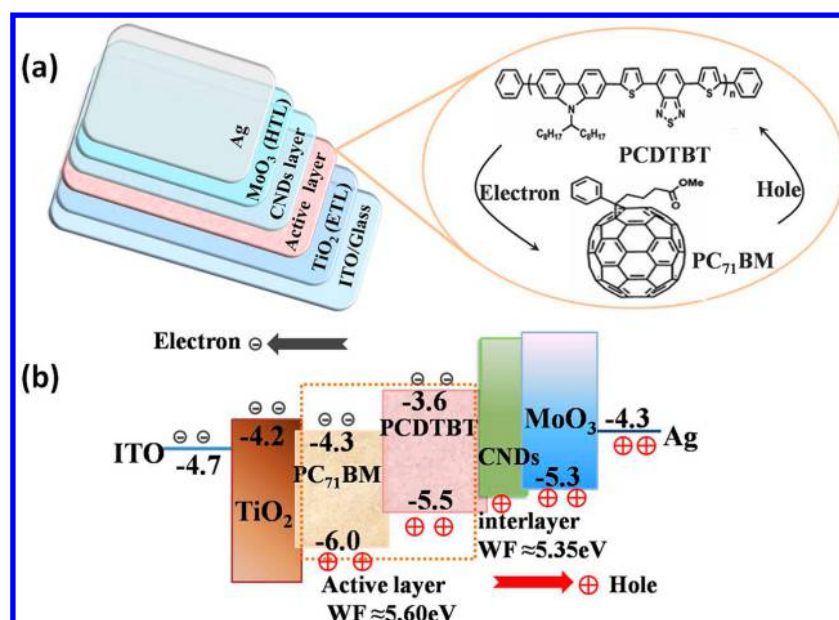


Figure 2. (a) Device structure of the inverted BHJ-OSCs. (b) Scheme of energy levels of the materials involved in inverted polymer solar cells.

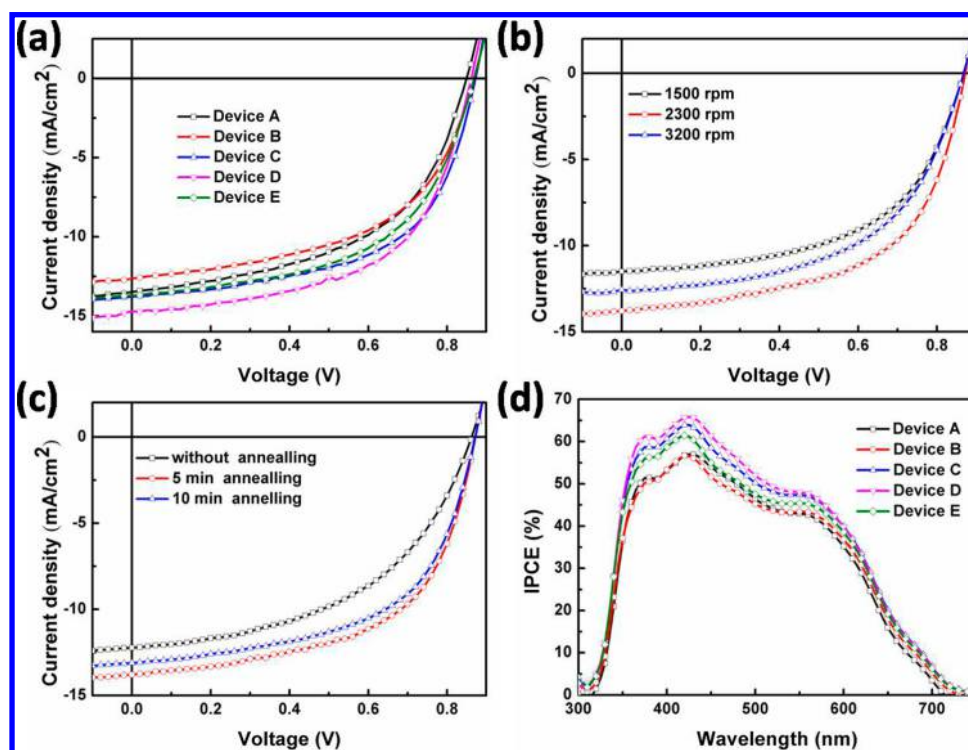


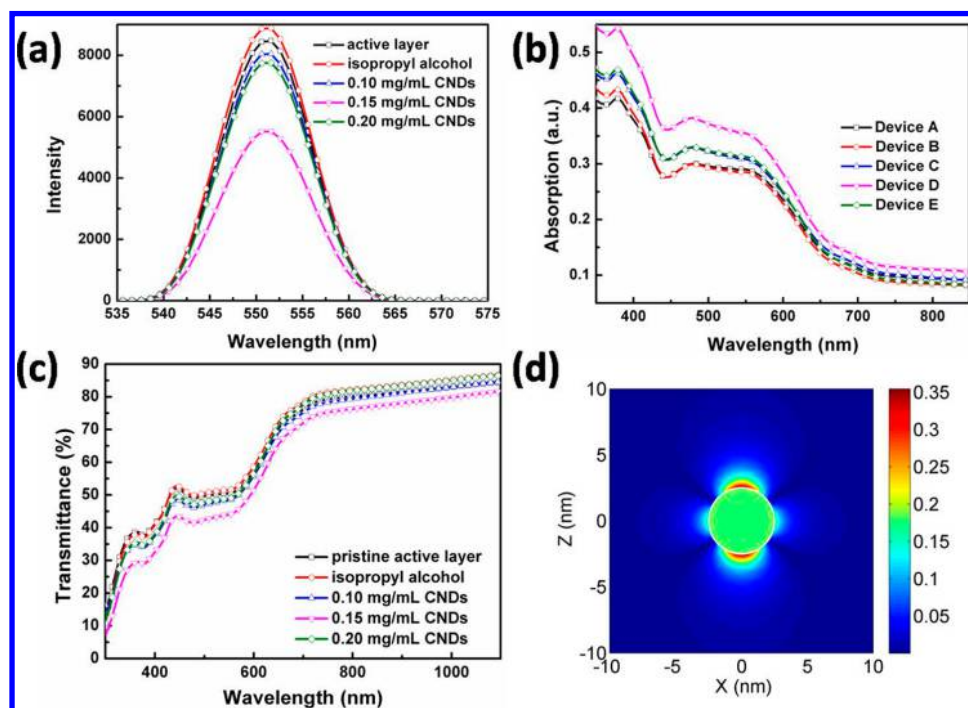
Figure 3. (a)  $J$ - $V$  characteristics of devices modified without and with various concentration of CNDs solution as interlayer. (b)  $J$ - $V$  characteristics of devices modified with different thickness (0.1 mg/mL) CNDs interlayer. (c)  $J$ - $V$  characteristics of devices modified with (0.1 mg/mL) CNDs interlayer with different annealing time, under AM1.5G illumination with the intensity of  $100 \text{ mW cm}^{-2}$  in ambient air. (d) IPCE of OSCs devices without and with different modifiers.

The WF of Au (5 eV) was chosen as a reference, the WF of pristine active layer and active layer/CNDs interlayer films were characterized by  $\text{WF} = 5 \text{ eV} - \text{WF}_{\text{Au-measure}} + \text{WF}_{\text{measure}}$ , and the work functions are 5.598 and 5.352 eV respectively.<sup>48,49</sup> Modification with CNDs interlayer slightly reduced the work function of active film, which decreased the energy barrier and thus promoted the hole extraction from organic layer to  $\text{MoO}_3$  HTL. The series resistance ( $R_s$ ) of device is defined by the slope of the  $J$ - $V$  curve at  $J_{sc} = 0$ .<sup>50</sup> The  $R_s$  is estimated to be

176.48 ohm for the Device A and 117.12 ohm for Device D, which contribute to the enhancement of FF from 51.79% to 56.91%. The decrease of  $R_s$  and improvement of conductivity of all modified devices were achieved, which enhanced charge transport capacity of  $\text{MoO}_3$  layer, leading to a better hole collection.<sup>51,52</sup> Device B modified with only isopropyl alcohol shows an increased FF of 52.83% but a decreased  $J_{sc}$  of  $12.64 \text{ mA cm}^{-2}$  and results in a decreased PCE of 5.795%. Therefore, the performance enhancement of devices with CNDs interlayer

**Table 1.** Key Photovoltaic Parameters, Including Short-Circuit Current Density ( $J_{sc}$ ), Open-Circuit Voltage ( $V_{oc}$ ), Power Conversion Efficiency (PCE), Fill Factor (FF), Series Resistance ( $R_s$ ), and Shunt Resistance ( $R_{sh}$ ) of All Fabricated OSCs

device	$V_{oc}$ (V)	$J_{sc}$ ( $\text{mA cm}^{-2}$ )	FF (%)	PCE (%)	$R_s$ (ohm)	$R_{sh}$ (ohm)
A	$0.85 \pm 0.01$	$13.49 \pm 0.11$	$51.74 \pm 0.02$	$5.93 \pm 0.13$	176.48	3799.70
B	$0.87 \pm 0.04$	$12.64 \pm 0.12$	$52.83 \pm 0.04$	$5.80 \pm 0.10$	174.43	4419.89
C	$0.87 \pm 0.02$	$13.79 \pm 0.08$	$56.91 \pm 0.03$	$6.84 \pm 0.14$	122.73	7710.79
D	$0.87 \pm 0.05$	$14.71 \pm 0.07$	$56.93 \pm 0.03$	$7.22 \pm 0.13$	117.12	7900.79
E	$0.86 \pm 0.01$	$13.70 \pm 0.07$	$54.65 \pm 0.02$	$6.51 \pm 0.11$	151.71	6326.96

**Figure 4.** (a) PL spectra of the pristine PCDTB:PC<sub>71</sub>BM, PCDTB:PC<sub>71</sub>BM/isopropyl alcohol, and PCDTB:PC<sub>71</sub>BM/CNDs interlayer with different concentration films. (b) Absorption spectrum of TiO<sub>2</sub>/PCDTBT:PC<sub>71</sub>BM thin film with various capped layer on glass substrate. (c) Transmission spectrum of TiO<sub>2</sub>/PCDTBT:PC<sub>71</sub>BM thin film with various capped layer on glass substrate. (d) Calculated field intensity around CNDs.

is mainly attributed to CNDs additive not isopropyl solution. Under the optimal condition, CNDs can uniformly disperse in the interfacial layer and thus increase the conductivity of polymer material; thus, the hole carriers own a better transport property. Meanwhile, a CNDs interlayer provided a better interfacial contact for the active layer and MoO<sub>3</sub> HTL, leading to an increase of FF. Moreover, the film might have better phase separation and continuous interpenetrating networks with further annealing after CNDs layer was spin-coated, which is beneficial to the efficiency enhancement of OSCs. The detailed photovoltaic data of all fabricated devices are summarized in Table 1, which are typically an average of 40 devices.

Beforehand, we have chosen 0.1 mg/mL CNDs solution spinning cast under 1500, 2300, and 3200 rpm for 18 s with the same preprocess to determine the best film-forming condition, and the corresponding thicknesses of interlayer are 6, 4, and 3 nm. Figure 3b shows the  $J$ - $V$  characteristics of cells with different thickness of CNDs interlayer. With a low rotation speed (1500 rpm), the CNDs interlayer is unduly thick and the quality of the film is relatively inferior, providing more chances for charge recombination, leading to a poor performance of OSCs. Under a high rpm (3200 rpm), 3 nm CNDs interlayer is too thin to validly increase conductivity and appropriately

adjust the roughness of the film. Under the 2300 rpm spin-coating condition, CNDs interlayer is ideal to be a modifier and forms a more closed contact with HTL, which is good for charge transfer and hole accumulation decrease. Additionally, we have investigated the best later annealing time of CNDs interlayer with Device C, which is shown in Figure 3c. Without a later annealing, the cells showed a poor PCE with a declined  $V_{oc}$ ,  $J_{sc}$ , and FF, indicating that a bad film quality of interlayer is harmful to the device performance. After 10 min annealing, the modified devices exhibited a slightly lower  $J_{sc}$  and FF, which have great impact on the overall PCEs. After 5 min later annealing, the photovoltaic devices indicated the highest efficiency, and the interlayer surface possesses the best feature and the active layers own an excellent phase separation scale, which accelerate the exciton dissociation, charge transport, and charge collection.

The incident photon-to-current efficiency (IPCE) spectra of devices with and without modified interlayer was measured with CrownTech QTest Station 1000 AD and shown in Figure 3d. It is found that the variation tendency of IPCE is similar to that of  $J_{sc}$  in Figure 3a. At a wavelength region of 340–700 nm, the CNDs modified devices fabricated at optimal conditions have much higher IPCE than the control devices especially from 360 to 560 nm. The IPCE of optimal Device D reaches

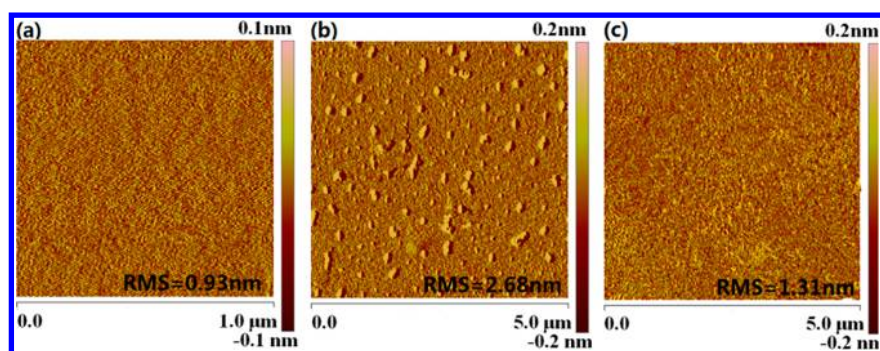


**Figure 5.** AFM morphology image of active layer film without and with modifier. (a) Active layer film without modifier, (b) active layer film modified with isopropyl alcohol, and (c) active layer film modified with optimal CNDs interlayer.

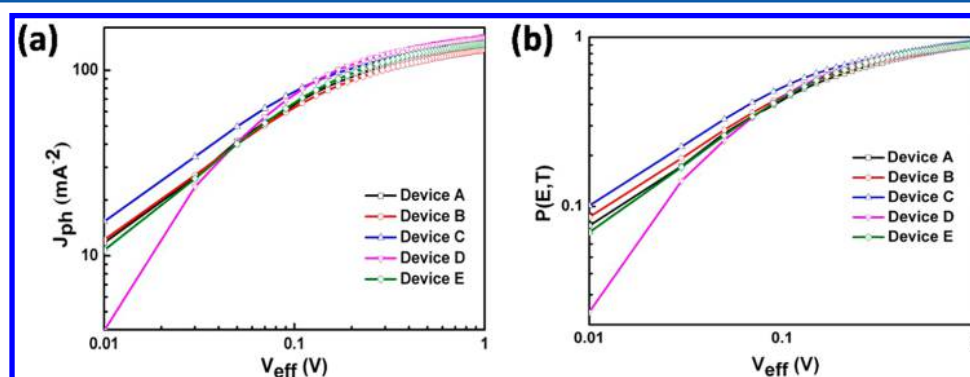


**Figure 6.** (a) Photocurrent density ( $J_{ph}$ ) as a function of the effective voltage ( $V_{eff}$ ) for control and optimal modified devices under constant incident light intensity. (b) Corresponding plots of  $P(E, T)$  with respect to the effective bias ( $V_{eff}$ ) in different devices.

66% at 440 nm. Thus, efficient charge transfer from active layer to CNDs can energetically boost charge dissociation and transport through assisting sweeping out inner excitons, and then the  $J_{sc}$  and FF can achieve a great improvement. As expected, Device B only modified with isopropyl alcohol was the worst one and was no better than control devices, which reveals that the performance improvement originated from incorporating CNDs.

To further investigate the role of CNDs, the photoluminescence (PL) spectrum of active layer without and with different concentration of CNDs was tested and is shown in Figure 4a. Pure PCDTBT:PC<sub>71</sub>BM film exhibits strong emission peak around 550 nm, which gradually decreases for the active layers capped by CNDs. Such a reduction confirmed the efficient charge transfer occurring between the polymer material and CNDs. As D–A materials form interpenetrating nets within active layer, among which there diffuse some individual islands, the precise fitted CNDs interlayer would connect these islands and form efficient charge transport paths, contributing to the charge carrier transfer. Additionally, PL measurement was also implemented for PCDTBT:PC<sub>71</sub>BM capped with only isopropyl alcohol, and not surprisingly, the composite film shows an increased peak around 550 nm compared to pure PCDTBT:PC<sub>71</sub>BM layer, which unravels that the efficient charge transport is really attributed to CNDs and not the solvent.

The efficiency of solar cells is dependent on the light absorption of active layer. To gain a deep insight into CNDs capped layer on the photon harvesting of active layer, the normalized UV–vis absorption spectra of the blend films were measured. Figure 4b shows the light-harvesting of TiO<sub>2</sub>/PCDTBT:PC<sub>71</sub>BM films with different kinds of capped layer.

The absorption of the CNDs-modified films in 350–550 nm is observed to be more enhanced than that of the unmodified film, which is in keeping with IPCE results in Figure 3d. With CNDs interlayer, a rougher interface contributes to incident light reflected and scattered into active layer, resulting in light absorption improvement. Figure 4c is the light transmittance spectra of active layer with different modifiers, which is in conformity with Figure 4b. To demonstrate the optical effect of CNDs on active layer, the electric field profile of CNDs was simulated using finite-difference time-domain (FDTD) methods. We set the size and shape of CNDs according to the TEM image (Figure 1). The theoretical analogue result of electric field at the wavelength of 500 nm is exhibited in Figure 4d, and the color scale corresponds with the magnitude of the increased intensity. It can be seen that the light intensity around CNDs was greatly enhanced, and the scattering and reflection effect could make a contribution to the increased light trapping.

To explore the variation of the film roughness caused by CNDs interlayer, atomic force microscopy (AFM) was used to study the morphologies of thin films. Figure 5 presents tapping-mode AFM images (surface area:  $5 \times 5 \mu\text{m}^2$ ) of pristine active layer film, active layer/isopropyl alcohol film, and active layer/CNDs (1.5 mg/mL) film. The root-mean-square (RMS) of pristine PCDTBT:PC<sub>71</sub>BM film is about 0.93 nm (Figure 5a). In addition, it is noteworthy that the RMS roughness of composite film incorporating isopropyl alcohol (Figure 5b) is 2.68 nm, which indicates an extremely uneven surface with anomalous hills compared to that obtained from Figure 5a, and the ridgy film surface will trap more charge carriers to cause a decreased  $J_{sc}$ . Consequently, the device processed with pure isopropyl alcohol modifier displays an extravagant roughness and leads to an inferior PCE, which is consistent with  $J-V$

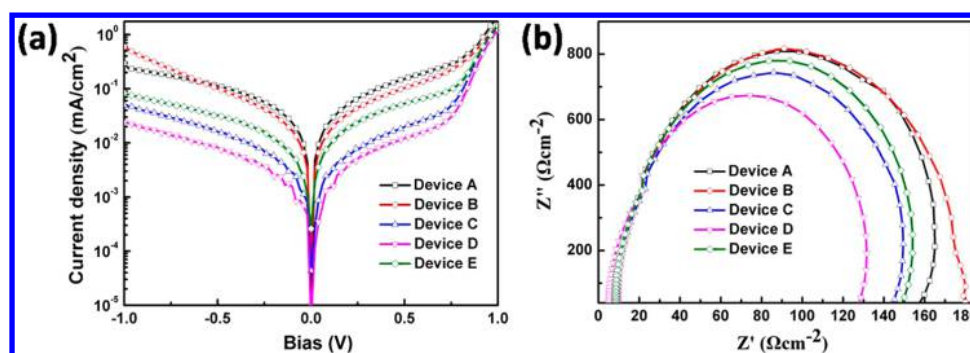


**Figure 7.** (a)  $J$ - $V$  characteristics of devices without and with different concentration of CNDS interlayer modification in the dark. (b) Nyquist plots of impedance spectra for OSCs devices with different concentration of CNDS interlayer modification in the dark.

results. Dramatically, the optimal CNDS interlayer at a specific condition roughens active layer mildly (RMS = 1.31 nm), presenting an obvious homogeneous terrain (Figure 5c). Generally, the evaporated thin MoO<sub>3</sub> HTL is comparatively uneven and incompact, and the leaky contact has great impact on resistivity. A moderate rougher film is beneficial for the interfacial contact between the photolayer and HTL due to the larger specific surface area contact after incorporating CNDS layer, accompanied by the diminished value of  $R_s$ .<sup>53</sup> A suitable capped layer uniformly roughens active layer surface and forms a charge transmission channel to improve hole transfer without destroying internal continuous interpenetrating network, which facilitates holes to be collected by anode and hinders hole-electron recombination.

To deeply understand the charge generation and separation process of the optimized OSCs, the photocurrent density dependence on the effective voltage ( $V_{\text{eff}}$ ) of cells was deduced and is shown in Figure 6a. Photocurrent density is defined as the difference between the current density  $J_L$  under illumination and the current density  $J_D$  in dark, and  $J_{\text{ph}} = J_L - J_D$ . The  $V_0$  is defined as the voltage when  $J_{\text{ph}} = 0$  mA/cm<sup>2</sup>.  $V_{\text{eff}}$  is determined as  $V_{\text{eff}} = V_0 - V$ , where  $V$  is the applied bias voltage.<sup>54</sup> It can be seen from Figure 6a that the photocurrent density nicely saturates at high  $V_{\text{eff}}$ , meaning that all photogenerated excitations are dissociated and extracted at sufficiently large reverse bias. Along with an increase of reverse bias,  $J_{\text{ph}}$  of the Device D saturated more rapidly than that of control device, suggesting that optimal devices could provide more effective charge carrier transfer.<sup>55</sup> The value of the saturation photocurrent density ( $J_{\text{sat}}$ ) is limited by total absorbed incident photons amount. Therefore,  $G_{\text{max}}$  could be calculated from  $J_{\text{sat}} = qG_{\text{max}}L$ , where  $q$  is the electronic charge and  $L$  is the thickness of active layer (100 nm). The values of  $G_{\text{max}}$  for the control device, solvent modified devices, and optimal device are  $9.599 \times 10^{27}$  m<sup>-3</sup> s<sup>-1</sup> ( $J_{\text{sat}} = 153.597$  A m<sup>-2</sup>),  $8.843 \times 10^{27}$  m<sup>-3</sup> s<sup>-1</sup> ( $J_{\text{sat}} = 141.491$  A m<sup>-2</sup>), and  $1.043 \times 10^{28}$  m<sup>-3</sup> s<sup>-1</sup> ( $J_{\text{sat}} = 166.951$  A m<sup>-2</sup>) respectively. Thus, a noticeable enhancement of  $G_{\text{max}}$  was achieved after incorporating the CNDS interlayer. The maximum absorption of incident photons determined the  $G_{\text{max}}$  that is to say, the light utilization of photoactive is more sufficient than that of the Device D, which could be well confirmed by the variation of absorption spectra without and with CNDS modified layer (Figure 4b). In fact, not all the photogenerated excitons can be dissociated into free carriers in OSCs. Hence, the relationship between  $J_{\text{ph}}$  and the exciton dissociation probability [ $P(E, T)$ ] can be expressed by a power law equation of  $J_{\text{ph}} \propto P^\alpha$ , where  $\alpha$  is the recombination parameter and the  $P(E, T)$  could be obtained from the ratio of

$J_{\text{ph}}/J_{\text{sat}}$ .<sup>56,57</sup> Under the short-circuit condition ( $V = 0$  V), Figure 6b shows that the value of  $P(E, T)$  rises to 88% for the optimized device, which slightly contributes to the dissociation probability increase of excitons. Employing CNDS interlayer not only increases the exciton generation but also plays a positive role in the hole collection by anode, achieving better photocurrent as shown in Table 1.<sup>58</sup>

The  $J$ - $V$  curves of all devices without and with various modifications in the dark are shown in Figure 7a. As expected, all the CNDS modified devices show a small leakage current at negative voltages, indicating that the introduction of interlayer could prevent the current from leak. Upon modifying with CNDS interlayer, the diode rectification ratios are moderately meliorated, indicating that CNDS interlayer increases the shunt resistance ( $R_{\text{sh}}$ ) for modified devices and achieves a more efficient charge separation, and the corresponding results are included in Table 1. Impedance spectroscopy has been proved to be an effective approach to investigate the charge carrier kinetics for optoelectronic devices. To further illuminate the photovoltaic performance enhancement of modified cells, impedance spectra were carried out at a frequency range from 10 Hz to 1 MHz.<sup>59</sup> Figure 7b presents the Nyquist curves of the impedance spectra for all fabricated devices. The semicircle's diameter in the diagram represents the impedance, and the larger diameter represents the larger impedance. Obviously, semicircle's diameter of devices modified with CNDS is smaller than control devices, which reveals the smaller  $R_s$  for optimized devices. Therefore, the bias is mostly applied on the photolayer and not on the resistance across the contacts, which is beneficial to minimize the lost current across the materials in contact.<sup>60,61</sup> A better contact between active layer and HTL has been achieved through CNDS interlayer, and this result is consistent with the  $R_s$  derived from  $J$ - $V$  curves (Figure 3a). Attributed to the CNDS interlayer, an optimal modification brings significant decline of impedance, and a decreased  $R_s$  and increased  $R_{\text{sh}}$  have been achieved in the modified devices, accounting for the improved FF as well as overall performance.

For the purpose of directly investigating the effect of CNDS interlayer on the hole transport property, we fabricated single-hole devices with the structure of ITO/MoO<sub>3</sub>/PCDTBT:PC<sub>71</sub>BM/CNDS layer/MoO<sub>3</sub>/Ag, and dark  $J$ - $V$  characteristics of all cells are exhibited in Figure 8. The dark  $J_{\text{sc}}$  of single-hole device based on the same structure as Device B was tested to confirm the performance improvement originating from CNDS instead of solvent. Apparently,  $J_{\text{sc}}$  of Device B stayed the same level as unmodified Device A, which is to say that only modification with isopropyl alcohol is of no

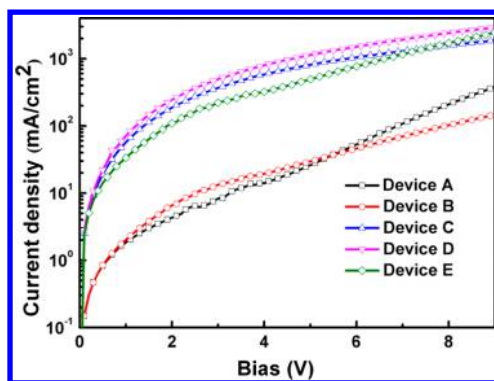


**Figure 8.**  $J$ - $V$  characteristics of hole-only devices without and with various concentrations of CNDs interlayer.

use to enhance the hole mobility.  $J_{sc}$  of all CNDs modified devices outclassed that of control devices in the dark. Under the same driving voltage without illumination,  $J_{sc}$  mainly depends on the holes' directional movement, and we could infer that modified devices indeed possess better hole transport capacity due to the good conductivity of CNDs. We made a realistic evaluation of hole mobility calculated from SCLC model to verify that CNDs interlayer could significantly improve the hole transport.<sup>62–64</sup> At an applied voltage of 1.5 V, corresponding to an electric field of  $10^5$  V  $cm^{-1}$  across the bulk of a 100 nm devices, apparent hole mobilities of  $3.34 \times 10^{-5}$ ,  $4.26 \times 10^{-5}$ ,  $1.27 \times 10^{-3}$ ,  $1.63 \times 10^{-3}$ , and  $7.09 \times 10^{-4}$   $cm^2$   $V^{-1}$   $s^{-1}$  have been computed for the devices without and with modifier, respectively. Thus, the hole transport properties of Device A and B would be retarded, leading to a charge recombination increase and  $J_{sc}$  decrease. Upon introducing CNDs interlayer, the hole mobility increased more than 1 order of magnitude, which is comparable to electron mobility, and a more balanced charge transport can be achieved in OSCs. These are strong evidence that hole transport capacity is largely enhanced by CNDs interlayer, thus confining the effects of space charge formation and mitigating the photocarriers loss from recombination, leading to a significant improvement of  $J_{sc}$ .

#### 4. CONCLUSION

In conclusion, CNDs were employed as interlayer between active layer and  $MoO_3$  HTL to achieve progress on efficiency of inverted OSCs. The dependence of CNDs concentrations on device performance was investigated, and PCEs of the corresponding inverted OSC devices reached 6.84%, 7.22%, and 6.51%, which presented an enhancement of 15.45%, 21.74%, and 9.73% compared to the control devices, respectively. The incorporation of CNDs interfacial layer is conducive to improve  $J_{sc}$  and FF because of the synergistic effect of the maximizing absorption of active layer, optimizing resistance, and improving charge transport property. Single carrier device investigation revealed that the efficient hole transport provided the increased average hole lifetime and collection with suppressed hole accumulation and bimolecular recombination in OSCs. Our work offers a facile method to improve efficiency of OSCs.

#### AUTHOR INFORMATION

##### Corresponding Authors

\*Tel.: +86 431 85168270. E-mail: guowb@jlu.edu.cn.

\*Tel.: +86 431 85168270.

#### Notes

The authors declare no competing financial interest.

#### ACKNOWLEDGMENTS

The authors are grateful to National Natural Science Foundation of China (61275035, 61370046, 11574110), Project of Science and Technology Development Plan of Jilin Province (20140101060JC, 20150519003JH), and the Opened Fund of the State Key Laboratory on Integrated Optoelectronics (IOSKL2013KF10) for the support of the work.

#### REFERENCES

- (1) Park, B. C.; Yun, S. H.; Cho, C. Y.; Kim, Y. C.; Shin, J. C.; Jeon, H. G.; Huh, Y. H.; Hwang, I. C.; Baik, K. Y.; Lee, Y. I.; et al. Surface Plasmon Excitation in Semitransparent Inverted Polymer Photovoltaic Devices and Their Applications as Label-free Optical Sensors. *Light: Sci. Appl.* **2014**, *3*, e222.
- (2) Huang, J.; Li, C. Z.; Chueh, C. C.; Liu, S. Q.; Yu, J. S.; Jen, A. K. Y. 10.4% Power Conversion Efficiency of ITO-free Organic Photovoltaics through Enhanced Light Trapping Configuration. *Adv. Energy Mater.* **2015**, *5*, 1500406.
- (3) Yusoff, A. R. M.; Kim, D.; Kim, H. P.; Shneider, F. K.; da Silva, W. J.; Jang, J. A High Efficiency Solution Processed Polymer Inverted Triple-Junction Solar Cell Exhibiting a Power Conversion Efficiency of 11.83%. *Energy Environ. Sci.* **2015**, *8*, 303–316.
- (4) Chen, H. Y.; Hou, J. H.; Zhang, S. Q.; Liang, Y. Y.; Yang, G. W.; Yang, Y.; Yu, L.; Wu, Y.; Li, G. Polymer Solar Cells with Enhanced Open-Circuit Voltage and Efficiency. *Nat. Photonics* **2009**, *3*, 649–653.
- (5) Li, G.; Zhu, R.; Yang, Y. Polymer Solar Cells. *Nat. Photonics* **2012**, *6*, 153–161.
- (6) Sudeep, P. K.; Early, K. T.; McCarthy, K. D.; Odoi, M. Y.; Barnes, M. D.; Emrick, T. Monodisperse Oligo(phenylene vinylene) Ligands on CdSe Quantum Dots: Synthesis and Polarization Anisotropy Measurements. *J. Am. Chem. Soc.* **2008**, *130*, 2384–2385.
- (7) Zhang, F. J.; Zhao, D. W.; Zhuo, Z. L.; Wang, H.; Xu, Z.; Wang, Y. S. Inverted Small Molecule Organic Solar Cells with Ca Modified ITO as Cathode and  $MoO_3$  Modified Ag as Anode. *Sol. Energy Mater. Sol. Cells* **2010**, *94*, 2416–2421.
- (8) Ma, H.; Yip, H. L.; Huang, F.; Jen, A. K. Y. Interface Engineering for Organic Electronics. *Adv. Funct. Mater.* **2010**, *20*, 1371–1388.
- (9) Wicklein, A.; Ghosh, S.; Sommer, M.; Wurthner, F.; Thelakkat, M. Self Assembly of Semiconductor Organogelator Nanowires for Photoinduced Charge Separation. *ACS Nano* **2009**, *3*, 1107–1114.
- (10) Kim, J. Y.; Lee, K.; Coates, N. E.; Moses, D.; Nguyen, T. Q.; Dante, M.; Heeger, A. J. Efficient Tandem Polymer Solar Cells Fabricated by All-Solution Processing. *Science* **2007**, *317*, 222–225.
- (11) Park, S. H.; Roy, A.; Beaupre, S.; Cho, S.; Coates, N.; Moon, J. S.; Moses, D.; Leclerc, M.; Lee, K.; Heeger, A. J. Bulk Heterojunction Solar Cells with Internal Quantum Efficiency Approaching 100%. *Nat. Photonics* **2009**, *3*, 297–302.
- (12) Zhang, F. J.; Xu, X. W.; Tang, W. H.; Zhang, J.; Zhuo, Z. L.; Wang, J.; Wang, J.; Xu, Z.; Wang, Y. S. Recent Development of the Inverted Configuration Organic Solar Cells. *Sol. Energy Mater. Sol. Cells* **2011**, *95*, 1785–1799.
- (13) Peunmans, P.; Yakimov, A.; Forrest, S. R. Small Molecular Weight Organic Thin-Film Photodetectors and Solar Cells. *J. Appl. Phys.* **2003**, *93*, 3693–3723.
- (14) Rim, S. B.; Zhao, S.; Scully, S. R.; McGehee, M. D.; Peunmans, P. An Effective Light Trapping Configuration for Thin-Film Solar Cells. *Appl. Phys. Lett.* **2007**, *91*, 243501–243503.
- (15) Ko, D. H.; Tumbleston, J. R.; Gadisa, A.; Aryal, M.; Liu, Y.; Lopez, R.; Samulski, E. T. Light-Trapping Nanostructures in Organic Photovoltaic Cells. *J. Mater. Chem.* **2011**, *21*, 16293–16303.
- (16) Kim, J. Y.; Kim, S. H.; Lee, H. H.; Lee, K.; Ma, W.; Gong, X.; Heeger, A. J. New Architecture for High-Efficiency Polymer Photovoltaic Cells Using Solution-Based Titanium Oxide as an Optical Spacer. *Adv. Mater.* **2006**, *18*, 572–576.

- (17) Chen, X.; Jia, B. H.; Zhang, Y. A.; Gu, M. Exceeding the Limit of Plasmonic Light Trapping in Textured Screen-Printed Solar Cells Using Al Nanoparticles and Wrinkle-like Graphene Sheets. *Light: Sci. Appl.* **2013**, *2*, e92.
- (18) Dennler, G.; Scharber, M. C.; Ameri, T.; Denk, P.; Forberich, K.; Waldauf, C.; Brabec, C. J. Design Rules for Donors in Bulk-Heterojunction Tandem Solar Cells towards 15% Energy-Conversion Efficiency. *Adv. Mater.* **2008**, *20*, 579–583.
- (19) Szarko, J. M.; Guo, J.; Rolczynski, B. S.; Chen, L. X. Current Trends in the Optimization of Low Band Gap Polymers in Bulk Heterojunction Photovoltaic Devices. *J. Mater. Chem.* **2011**, *21*, 7849–7857.
- (20) He, Z.; Xiao, B.; Liu, F.; Wu, H.; Yang, Y.; Xiao, S.; Wang, C.; Russell, T. P.; Cao, Y. Single-Junction Polymer Solar Cells with High Efficiency and Photovoltage. *Nat. Photonics* **2015**, *9*, 174–179.
- (21) Su, Y. H.; Ke, Y. F.; Cai, S. L.; Yao, Q. Y. Surface Plasmon Resonance of Layer-by-layer Gold Nanoparticles Induced Photoelectric Current in Environmentally-friendly Plasmon-sensitized Solar Cell. *Light: Sci. Appl.* **2012**, *1*, e14.
- (22) Dayal, S.; Kopidakis, N.; Olson, D. C.; Ginley, D. S.; Rumbles, G. Photovoltaic Devices with a Low Band Gap Polymer and CdSe Nanostructures Exceeding 3% Efficiency. *Nano Lett.* **2010**, *10*, 239–242.
- (23) Weickert, J.; Dunbar, R. B.; Hesse, H. C.; Wiedemann, W.; Schmidt-Mende, L. Nanostructured Organic and Hybrid Solar Cells. *Adv. Mater.* **2011**, *23*, 1810–1828.
- (24) Van Duren, J. K. J.; Yang, X. N.; Loos, J.; Bulle Liewma, C. W. T.; Sieval, A. B.; Hummelen, J. C.; Janssen, R. A. J. Relating the Morphology of Poly(*p*-phenylene vinylene)/Methanofullerene Blends to Solar Cell Performance. *Adv. Funct. Mater.* **2004**, *14*, 425–434.
- (25) Zhang, F. L.; Jespersen, K. G.; Bjorstrom, C.; Svensson, M.; Andersson, M. R.; Sundstrom, V.; Magnusson, K.; Moons, E.; Yartsev, A.; Inganäs, O. Influence of Solvent Mixing on the Morphology and Performance of Solar Cells Based on Polyfluorene Copolymer/Fullerene Blends. *Adv. Funct. Mater.* **2006**, *16*, 667–674.
- (26) Hiorns, R. C.; De Bettignies, R.; Leroy, J.; Bailey, S.; Firon, M.; Senten, C.; Khoukh, A.; Preud'homme, H.; Dagron-Lartigau, C. High Molecular Weights, Polydispersities, and Annealing Temperatures in The Optimization of Bulk-Heterojunction Photovoltaic Cells Based on Poly(3-hexylthiophene) or Poly(3-butylthiophene). *Adv. Funct. Mater.* **2006**, *16*, 2263–2273.
- (27) Hoppe, H.; Niggemann, M.; Winder, C.; Kraut, J.; Heisgen, R.; Hinsch, A.; Meissner, D.; Sariciftci, N. S. Nanoscale Morphology of Conjugated Polymer/Fullerene-Based Bulk-Heterojunction Solar Cells. *Adv. Funct. Mater.* **2004**, *14*, 1005–1011.
- (28) Ma, W.; Yang, C.; Gong, X.; Lee, K. A.; Heeger, J. Thermally Stable, Efficient Polymer Solar Cells with Nanoscale Control of The Interpenetrating Network Morphology. *Adv. Funct. Mater.* **2005**, *15*, 1617–1622.
- (29) Shuttle, C. G.; O'Regan, B.; Ballantyne, A. M.; Nelson, J.; Bradley, D. D. C.; Durrant, J. R. Bimolecular Recombination Losses in Polythiophene: Fullerene Solar Cells. *Phys. Rev. B: Condens. Matter Mater. Phys.* **2008**, *78*, 113201.
- (30) Mihailetchi, V. D.; Wildeman, J.; Blom, P. W. M. Space-Charge Limited Photocurrent. *Phys. Rev. Lett.* **2005**, *94*, 126602.
- (31) Yip, H. L.; Jen, A. K. Y. Recent Advances in Solution-Processed Interfacial Materials for Efficient and Stable Polymer Solar Cells. *Energy Environ. Sci.* **2012**, *5*, 5994–6011.
- (32) Zhu, Y.; Xu, X.; Zhang, L.; Chen, J.; Cao, Y. High Efficiency Inverted Polymeric Bulk-Heterojunction Solar Cells with Hydrophilic Conjugated Polymers as Cathode Interlayer on ITO. *Sol. Energy Mater. Sol. Cells* **2012**, *97*, 83–88.
- (33) Zuo, L. J.; Jiang, X. X.; Xu, M. S.; Yang, L. G.; Nan, Y. X.; Yan, Q. X.; Chen, H. Z. Enhancement of Short Current Density in Polymer Solar Cells with Phthalocyanine Tin (IV) Dichloride as Interfacial Layer. *Sol. Energy Mater. Sol. Cells* **2011**, *95*, 2664–2669.
- (34) Yusoff, A. R.; Kim, M. D.; Kim, H. P.; Shneider, F. K.; da Silva, W. J.; Jang, J. A High Efficiency Solution Processed Polymer Inverted Triple-Junction Solar Cell Exhibiting A Power Conversion Efficiency of 11.83%. *Energy Environ. Sci.* **2015**, *8*, 303–316.
- (35) Lu, L.; Xu, T.; Jung, I. H.; Yu, L. Match the Interfacial Energy Levels Between Hole Transport Layer and Donor Polymer To Achieve High Solar Cell Performance. *J. Phys. Chem. C* **2014**, *118*, 22834–22839.
- (36) Sun, Y.; Takacs, C. J.; Cowan, S. R.; Seo, J. H.; Gong, X.; Roy, A.; Heeger, A. J. Efficient, Air-Stable Bulk Heterojunction Polymer Solar Cells Using MoO<sub>3</sub> as the Anode Interfacial Layer. *Adv. Mater.* **2011**, *23*, 2226–2230.
- (37) Irwin, M. D.; Buchholz, D. B.; Hains, A. W.; Chang, R. P. H.; Marks, T. J. p-Type Semiconducting Nickel Oxide as an Efficiency-Enhancing Anode Interfacial Layer in Polymer Bulk-Heterojunction Solar Cells. *Proc. Natl. Acad. Sci. U. S. A.* **2008**, *105*, 2783–2787.
- (38) Lee, K. S.; Lee, J. A.; Mazor, B. A.; Forrest, S. R. Transforming the Cost of Solar-to-Electrical Energy Conversion: Integrating Thin-film GaAs Solar Cells with Nontracking Mini-Concentrators. *Light: Sci. Appl.* **2015**, *4*, e288.
- (39) Irwin, M. D.; Buchholz, D. B.; Hains, A. W.; Chang, R. P. H.; Marks, T. J. P-Type Semiconducting Nickel Oxide as an Efficiency-Enhancing Anode Interfacial Layer in Polymer Bulk-heterojunction Solar Cells. *Proc. Natl. Acad. Sci. U. S. A.* **2008**, *105*, 2783–2787.
- (40) Qu, S.; Liu, X.; Guo, X.; Chu, M.; Zhang, L.; Shen, D. Amplified Spontaneous Green Emission and Lasing Emission from Carbon Nanoparticles. *Adv. Funct. Mater.* **2014**, *24*, 2689–2695.
- (41) Zhang, X. Y.; Li, Z. Q.; Zhang, Z. H.; Liu, C. Y.; Li, J. F.; Guo, W. B.; Qu, S. N. Employing Easily Prepared Carbon Nanoparticles To Improve Performance of Inverted Organic Solar Cells. *ACS Sustainable Chem. Eng.* **2016**, *4*, 2359–2365.
- (42) Zhang, X. Y.; Zheng, K. Z.; Liu, C. Y.; Li, H.; Li, Z. Q.; Li, J. F.; He, Y. Y.; Guo, W. B.; Shen, L.; Ruan, S. P. Enhancing the Light-Harvesting and Charge Transport Properties of Polymer Solar Cells by Embedding NaLuF<sub>4</sub>:Yb,Tm Nanorods. *RSC Adv.* **2015**, *5*, 32891–32896.
- (43) Qu, S.; Wang, X.; Lu, Q.; Liu, X.; Wang, L. A Biocompatible Fluorescent Ink Based on Water-Soluble Luminescent Carbon Nanodots. *Angew. Chem.* **2012**, *51*, 12381–12384.
- (44) Holman, Z. C.; De Wolf, S. D.; Ballif, C. Improving Metal Reflectors by Suppressing Surface Plasmon Polaritons: a Priori Calculation of the Internal Reflectance of a Solar Cell. *Light: Sci. Appl.* **2013**, *2*, e106.
- (45) Li, Z. Q.; Li, S. J.; Zhang, Z. H.; Zhang, X. Y.; Li, J. F.; Liu, C. Y.; Shen, L.; Guo, W. B.; Ruan, S. P. Enhanced Electron Extraction Capability of Polymer Solar Cells via Modifying the Cathode Buffer Layer with Inorganic Quantum Dots. *Phys. Chem. Chem. Phys.* **2016**, *18*, 11435–11442.
- (46) Chen, H.; Hou, J.; Zhang, S.; Liang, Y.; Yang, G.; Yang, Y.; Yu, L.; Wu, Y.; Li, G. Polymer Solar Cells with Enhanced Open-Circuit Voltage and Efficiency. *Nat. Photonics* **2009**, *3*, 649–653.
- (47) Scharber, M. C.; Muhlbacher, D.; Koppe, M.; Denk, P.; Waldauf, C.; Heeger, A. J.; Brabec, C. J. Design Rules for Donors in Bulk-heterojunction Solar Cells—Towards 10% Energy-Conversion Efficiency. *Adv. Mater.* **2006**, *18*, 789–794.
- (48) Liu, X.; Wen, W.; Bazan, G. C. Post-deposition Treatment of an Arylated-carbazole Conjugated Polymer for Solar Cell Fabrication. *Adv. Mater.* **2012**, *24*, 4505–4510.
- (49) Li, X. C.; Xie, F. X.; Zhang, S. Q.; Hou, J. H.; Choy, W. C. MoO<sub>3</sub> and V<sub>2</sub>O<sub>5</sub> as Hole and Electron Transport Layers Through Functionalized Intercalation in Normal and Inverted Organic Optoelectronic Devices. *Light: Sci. Appl.* **2015**, *4*, e273.
- (50) Brabec, C. J.; Dyakonov, V.; Parisi, J. S.; Sariciftci, N. S. *Organic Photovoltaics Concepts and Realization*; Springer: Berlin, 2003.
- (51) Mihailetchi, V. D.; Wildeman, J.; Blom, P. W. M. Space-Charge Limited Photocurrent. *Phys. Rev. Lett.* **2005**, *94*, 126602.
- (52) Qu, S.; Wang, X.; Lu, Q.; Liu, X.; Wang, L. A Biocompatible Fluorescent Ink Based on Water-Soluble Luminescent Carbon Nanodots. *Angew. Chem., Int. Ed.* **2012**, *51*, 12215–12218.
- (53) Xu, J.; Voznyy, O.; Comin, R.; Gong, X. W.; Walters, G.; Liu, M.; Kanjanaboos, P.; Lan, X. H.; Sargent, E. H. Cross-linked Remote-

Doped Hole-Extracting Contacts Enhance Stability under Accelerated Lifetime Testing in Perovskite Solar Cells. *Adv. Mater.* **2016**, *28*, 2807–2805.

(54) Guo, W. B.; Zheng, K. Z.; Xie, W. F.; Sun, L.; Shen, L.; Liu, C. Y.; He, Y. Y.; Zhang, Z. H. Efficiency Enhancement of Inverted Polymer Solar Cells by Doping NaYF<sub>4</sub>:Yb<sup>3+</sup>, Er<sup>3+</sup> Nanocomposites in PCDTBT:PCBM Active Layer. *Sol. Energy Mater. Sol. Cells* **2014**, *124*, 126–132.

(55) Wang, D. H.; Kim, D. Y.; Choi, K.W. J.; Seo, H.; Im, S. H.; Park, J. H.; Park, O. O.; Heeger, A. J. Enhancement of Donor–Acceptor Polymer Bulk Heterojunction Solar Cell Power Conversion Efficiencies by Addition of Au Nanoparticles. *Angew. Chem., Int. Ed.* **2011**, *50*, 5519–5523.

(56) Fung, D. D. S.; Qiao, L. F.; Choy, W. C. H.; Wang, C. D.; Sha, W. E.; Xie, I. F. X.; He, S. L. Optical and Electrical Properties of Efficiency Enhanced Polymer Solar Cells with Au Nanoparticles in a PEDOT:PSS Layer. *J. Mater. Chem.* **2011**, *21*, 16349–16356.

(57) Kosten, E. D.; Atwater, J. H.; Parsons, J.; Polman, A.; Atwater, H. A. Highly Efficient GaAs Solar Cells by Limiting Light Emission Angle. *Light: Sci. Appl.* **2013**, *2*, e45.

(58) Wang, C. C. D.; Choy, W. C. H.; Duan, C.; Fung, D. D. S.; Sha, W. E. I.; Xie, F. X.; Huang, F.; Cao, Y. Optical and Electrical Effects of Gold Nanoparticles in the Active Layer of Polymer Solar Cells. *J. Mater. Chem.* **2012**, *22*, 1206–1211.

(59) Garcia-Belmonte, G.; Munar, A.; Barea, E. M.; Bisquert, J.; Ugarte, I.; Pacios, R. Charge Carrier Mobility and Lifetime of Organic Bulk Heterojunctions Analyzed by Impedance Spectroscopy. *Org. Electron.* **2008**, *9*, 847–851.

(60) Kim, G. H.; Song, H. K.; Kim, J. Y. The Effect of Introducing Buffer Layer to Polymer Solar Cells on Cell Efficiency. *Sol. Energy Mater. Sol. Cells* **2011**, *95*, 1119–1122.

(61) Perrier, G.; de Bettignies, R.; Berson, S.; Lemaitre, N.; Guillerez, S. Impedance Spectrometry of Optimized Standard and Inverted P3HT-PCBM Organic Solar Cells. *Sol. Energy Mater. Sol. Cells* **2012**, *101*, 210–216.

(62) Lepage, D.; Jimenez, A.; Beauvais, J.; Dubowski, J. J. Conic Hyperspectral Dispersion Mapping Applied to Semiconductor Plasmonics. *Light: Sci. Appl.* **2012**, *1*, e28.

(63) Taylor, R. A.; Otanicar, T.; Rosengarten, G. Nanofluid-Based Optical Filter Optimization For PV/T Systems. *Light: Sci. Appl.* **2012**, *1*, e34.

(64) Edwards, C.; Arbabi, A.; Popescu, G.; Goddard, L. L. Optically Monitoring and Controlling Nanoscale Topography During Semiconductor Etching. *Light: Sci. Appl.* **2012**, *1*, e30.